European Journal of Radiology 85 (2016) 1613–1621

Contents lists available at ScienceDirect

European Journal of Radiology

journal homepage: www.elsevier.com/locate/ejrad

Automatic segmentation of abdominal organs and adipose tissue compartments in water-fat MRI: Application to weight-loss in obesity

Jun Shen[a,b], Thomas Baum[b], Christian Cordes[b], Beate Ott[c], Thomas Skurk[c,d], Hendrik Kooijman[e], Ernst J. Rummeny[b], Hans Hauner[c,d], Bjoern H. Menze[a,1], Dimitrios C. Karampinos[b,*,1]

[a] Department of Computer Science, Technische Universität München, Munich, Germany
[b] Department of Diagnostic and Interventional Radiology, Klinikum rechts der Isar, Technische Universität München, Munich, Germany
[c] Else Kröner Fresenius Center for Nutritional Medicine, Klinikum rechts der Isar, Technische Universität München, Munich, Germany
[d] ZIEL Research Center for Nutrition and Food Sciences, Technische Universität München, Germany
[e] Philips Healthcare, Hamburg, Germany

ARTICLE INFO

Article history:
Received 8 April 2016
Received in revised form 26 May 2016
Accepted 6 June 2016

Keywords:
Subcutaneous adipose tissue (SAT)
Visceral adipose tissue (VAT)
Automatic image segmentation
Water-fat magnetic resonance imaging (MRI)
Weight loss

ABSTRACT

Purpose: To develop a fully automatic algorithm for abdominal organs and adipose tissue compartments segmentation and to assess organ and adipose tissue volume changes in longitudinal water-fat magnetic resonance imaging (MRI) data.
Materials and methods: Axial two-point Dixon images were acquired in 20 obese women (age range 24–65, BMI 34.9 ± 3.8 kg/m^2) before and after a four-week calorie restriction. Abdominal organs, subcutaneous adipose tissue (SAT) compartments (abdominal, anterior, posterior), SAT regions along the feet-head direction and regional visceral adipose tissue (VAT) were assessed by a fully automatic algorithm using morphological operations and a multi-atlas-based segmentation method.
Results: The accuracy of organ segmentation represented by Dice coefficients ranged from 0.672 ± 0.155 for the pancreas to 0.943 ± 0.023 for the liver. Abdominal SAT changes were significantly greater in the posterior than the anterior SAT compartment ($-11.4\% \pm 5.1\%$ versus $-9.5\% \pm 6.3\%$, $p < 0.001$). The loss of VAT that was not located around any organ ($-16.1\% \pm 8.9\%$) was significantly greater than the loss of VAT 5 cm around liver, left and right kidney, spleen, and pancreas ($p < 0.05$).
Conclusion: The presented fully automatic algorithm showed good performance in abdominal adipose tissue and organ segmentation, and allowed the detection of SAT and VAT subcompartments changes during weight loss.

1. Introduction

Obesity has become a major health issue, as an expanded adipose tissue accounts substantially to the risk for diabetes (by 44%), for ischemic heart disease (by 23%) and for cancer (by 7%–41%). In particular, the accumulation of abdominal adipose tissue (AAT) and organ fat plays an important role in the risk of obesity-related diseases. Lifestyle changes such as exercise programs or dietary interventions have been shown to produce weight loss and to significantly decrease the risk of obesity-related diseases [1]. Therefore, there is a growing interest in investigating the association between weight loss and changes of different adipose tissue compartments and in defining effective lifestyle intervention strategies for the prevention of obesity-related diseases in different patient groups [2].

Magnetic resonance imaging (MRI) is being increasingly used for non-invasively and accurately assessing adipose tissues and monitoring changes of different adipose tissue compartments after lifestyle interventions [3–5]. Specifically, the reduction of SAT and VAT volume or organ fat content has been investigated during interventions. Earlier studies used to estimate the SAT and VAT in the human body by using a single MRI slice, while a recent study showed that a single slice (L4-L5) poorly predicts SAT and VAT volume changes in general [6]. In addition, different compartments of SAT (e.g. anterior versus posterior and deep versus superficial) [7–9] and different compartments of VAT (e.g. intraperitoneal

* Corresponding author at: Department of Diagnostic and Interventional Radiology, Klinikum rechts der Isar, Ismaninger Str. 22, 81675 Munich, Germany.
E-mail address: dimitrios.karampinos@tum.de (D.C. Karampinos).
[1] equally contributed senior authors.

http://dx.doi.org/10.1016/j.ejrad.2016.06.006
0720-048X/

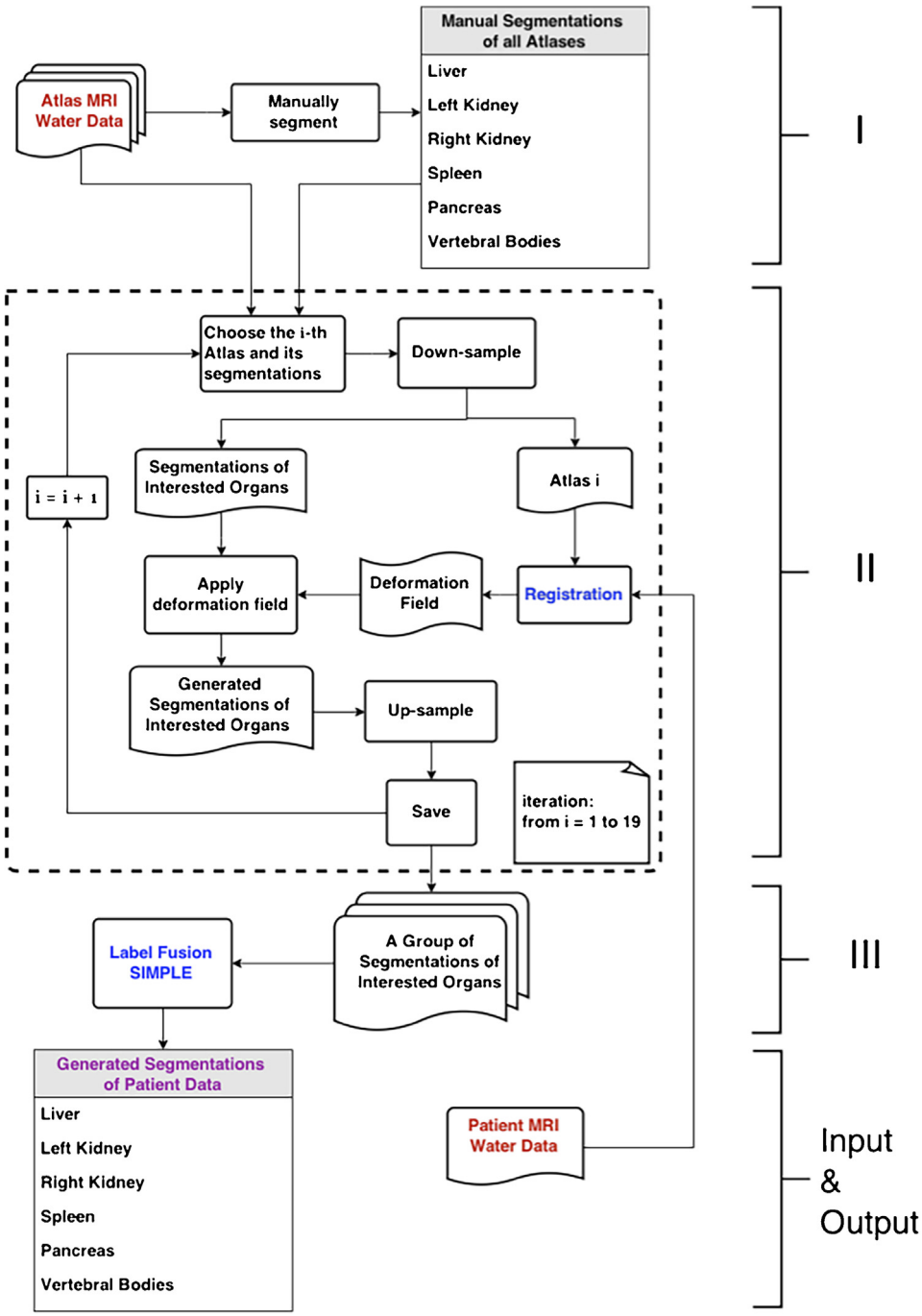

Fig. 1. Flow chart of the fully automatic organ segmentation approach: (I) atlas datasets consisted of 19 MRI water-only data. The labels of interested organs were generated for atlas datasets. (II) Group-wise registration was performed to normalize all atlases to the patient spatial coordinate system. The output of each registration was a deformation field, which was then applied to normalize the organ labels of atlas to patient space. (III) The normalized labels were resampled and fused to compute the final segmentation of interested organ of patient dataset.

versus retroperitoneal) [10,11] have been shown to have distinct metabolic properties and responses after interventions. Finally, the changes of organ volume and fat content in liver and pancreas after interventions have been of particular interest after interventions in obese subjects [12].

Chemical shift encoding-based water-fat MRI can separate water and fat signals relying on their chemical shift difference. Chemical shift encoding-based water-fat MRI has been recently emerging as a reliable method to generate co-registered water and fat images and measure fat content throughout the body [13]. However, the rapid and accurate extraction of SAT and VAT volume and organ fat content requires the combination of water-fat MRI with a reliable image analysis methodology [14]. The automatic method of localization and quantification of adipose tissue throughout the body is a long standing field of interest in image processing, as manual segmentation by a specialist is a tedious and time-consuming task, and the result directly depends on the specialist's experience and knowledge of anatomy [15–19]. Semi-automatic segmentation is more efficient than manual segmentation. However, semi-automatic segmentation still requires a moderate level of user interaction and cannot process large datasets efficiently. A fully automatic approach with robust performance is highly attrac-

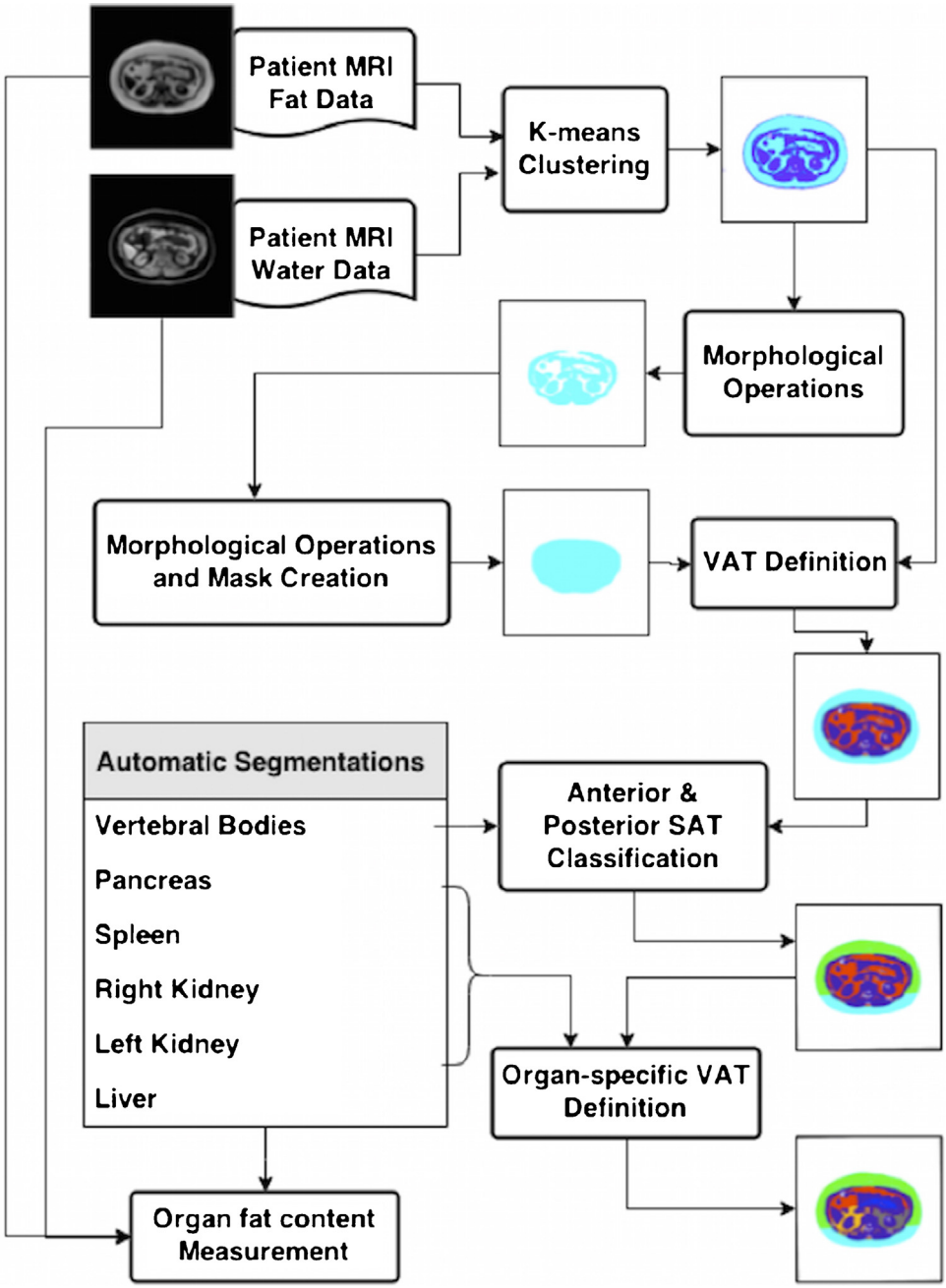

Fig. 2. Flow chart of AAT classification: VAT and SAT were determined from water and fat data by k-means clustering and morphological operations. According to the locations of vertebral bodies from automatic segmentation procedure, the abdominal SAT was further classified into anterior and posterior SAT. Meanwhile, organ-specific VAT was measured by means of organ labels.

tive and can significantly accelerate the segmentation workflow. In a previous study, a knowledge-based method was presented using statistical shape models (SSM) of the abdomen to distinguish different components of AAT [20]. However, the accuracy of such methods can depend on the specialist creating the average SSM of the abdomen. In some cases, an approximate shape model was used to localize organs [21]. In another recent study, an intra-subject registration-based segmentation method was introduced measuring SAT, VAT and the fat content of some organs [22]. However, the method was only applied for the assessment of the efficacy of the intervention in a longitudinal study. Most of the available automatic methods are limited to the classification of AAT into SAT and VAT and cannot characterize the regional distribution of SAT and VAT and quantify compartments of SAT and VAT.

The present work proposes a fully automatic multi-atlas-based approach for abdominal organ segmentation and regional adipose tissue analysis based on water-fat MRI data. The method was tested using MRI datasets from 20 obese patients who underwent MRI scans before and after a 4-week dietary intervention, and the performance of the organ segmentation was validated against manual segmentation as reference standard.

2. Materials and methods

2.1. Subjects and dietary intervention

The present human intervention study was carried out at the Human Study Center (HSC) of the Else Kröner-Fresenius-Center of

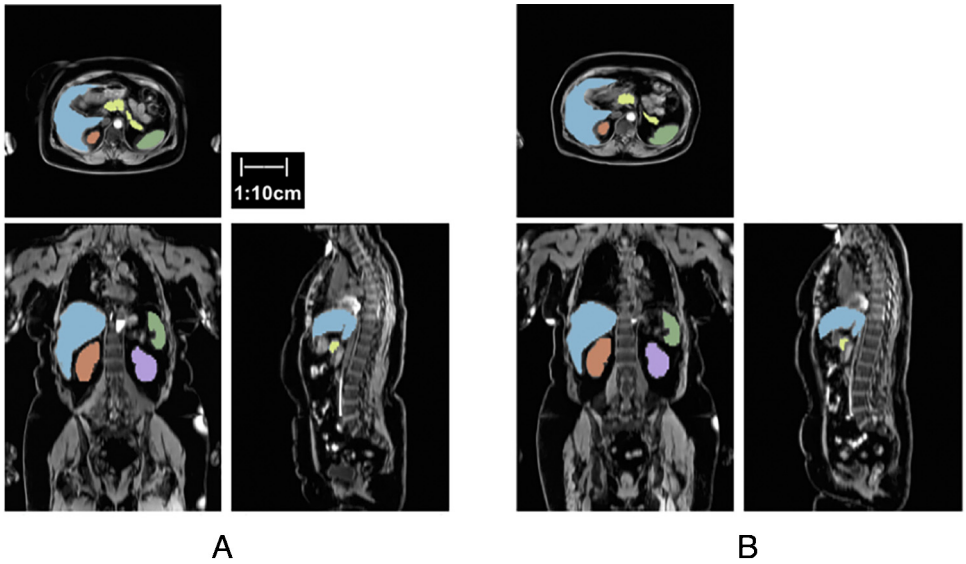

Fig. 3. Organ segmentation for one patient scanned before (A) and after (B) dietary intervention: liver (blue), spleen (green), right kidney (red), left kidney (purple) and pancreas (khaki).

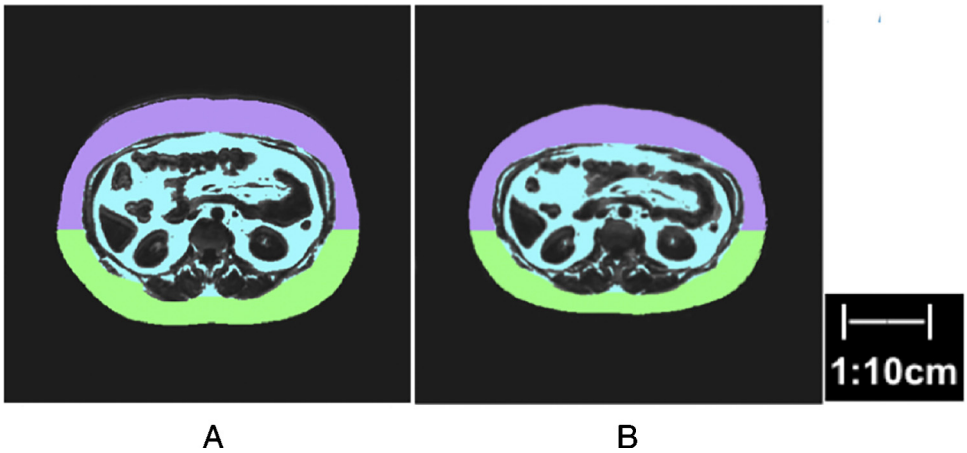

Fig. 4. SAT and VAT segmentation for one patient scanned before (A) and after (B) dietary intervention: anterior SAT (purple), posterior SAT (light green) and VAT (blue).

Nutritional Medicine (Technische Universität München, Germany), as previously also described in [3]. The study was approved by the ethical commission of the Faculty of Medicine of the Technische Universität München, Germany (#5499/12) and was registered in the German Clinical Trial Register (DRKS00006210). Informed written consent was obtained from the participants. After recruitment, twenty obese, non-smoking women (age range 24–65, BMI $34.9 \pm 3.8\,kg/m^2$) underwent a defined dietary intervention using a formula diet (four portions Modifast per day each containing 200 kcal, kindly provided by Nutrition Sante SAS, Revel, France) with a total daily energy intake of 800 kcal and additional 200 g of vegetables (raw or cooked without fat) for 28 days. MRI examinations were performed one day before the start and one day after the end of the dietary intervention but in the afternoons, so the participants were not fasting anymore.

2.2. MRI measurements

The abdominal region of the subjects was scanned on a 3T scanner (Ingenia; Philips Healthcare, Best, Netherlands, software release 4.1.3) using a 16-channel anterior coil array and a built-in-table 12-channel posterior coil array. Chemical shift encoding-based water-fat imaging was performed using a two-point Dixon technique. Specifically, axial two-point Dixon images based on a 3D spoiled gradient echo sequence (with non-flyback gradients) were acquired using two stacks with identical imaging parameters: TR = 4 ms, TE1/TE2 = 1.32/2.6 ms, flip angle = 10°, bandwidth = 1004 Hz/pixel, 332×220 acquisition matrix size, FOV = $500 \times 446\,mm^2$, acquisition voxel size = $1.5 \times 2.0\,mm^2$, slice thickness = 5 mm, 44 slices per stack, parallel imaging using SENSE with a reduction factor R = 2.5 and reconstruction voxel size = $0.98 \times 0.98\,mm^2$. The two stacks were aligned to cover the entire abdominal region starting at the top of the liver. The acquisition time for each stack was 10.6 s and the scanning of each stack was performed in a single breath-hold. Water and fat images were separated online on the scanner using a complex-based water-fat separation routine (mDixon algorithm), considering the presence of multiple peaks in the fat spectrum and correcting for eddy current effects [23].

40 MRI datasets were collected from the 20 obese patients who underwent the MRI scanning before and after a 4-week dietary intervention. Namely, 20 MRI datasets were acquired from patients before dietary intervention and the other 20 MRI datasets were acquired from patients after dietary intervention.

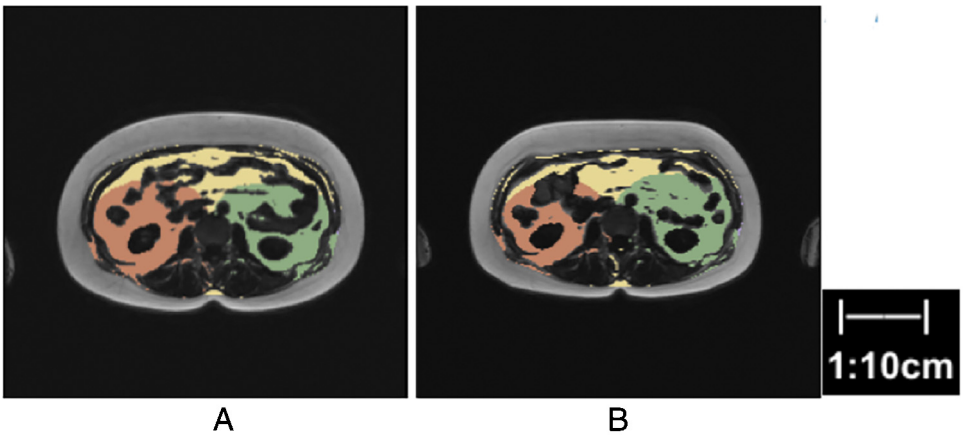

Fig. 5. Organ-specific VAT classification for one patient scanned before (A) and after (B) dietary intervention: VAT around right kidney in 5 cm (red), VAT around left kidney in 5 cm (green) and VAT not around any organs (yellow).

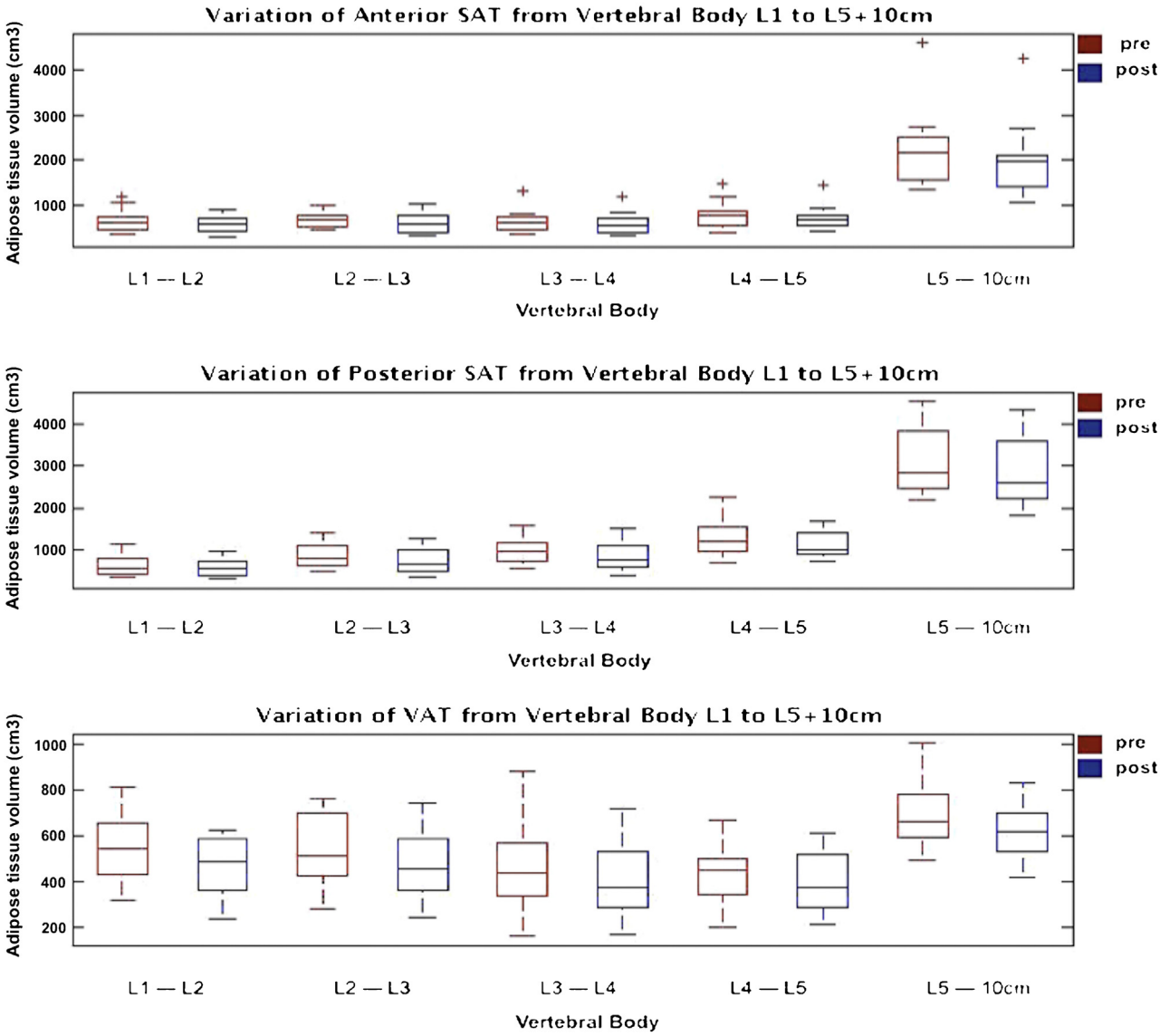

Fig. 6. SAT and VAT volume variation along the locations of vertebral bodies L1 to 10 cm downward from L5. Red and blue boxplots represent volume of adipose tissue from patients before and after dietary intervention, respectively.

Table 1
SAT changes for compartments (abdominal, anterior, posterior) and regions (L1-2, L2-3, L3-4, L4-5, L5-caudal). The "p-values for Δ" indicate statistically significant differences between baseline and follow-up SAT for the corresponding compartment or region. The "p-values for anterior vs. posterior" indicate statistically significant differences between ΔSAT of the anterior vs. posterior compartment of the different regions.

ΔSAT	absolute [cm^3]	relative [%]	p-value for Δ	p-value for anterior vs. posterior
abdominal	−1518.7 ± 632.8	−10.8 ± 4.2	<0.001	
anterior	−484.1 ± 339.5	−9.5 ± 6.3	<0.001	<0.001
posterior	−1034.6 ± 431.7	−11.4 ± 5.1	<0.001	
L1-2 abdominal	−101.7 ± 183.5	−6.6 ± 13.5	0.020	
L1-2 anterior	−57.8 ± 117.5	−7.8 ± 17.2	0.038	0.454
L1-2 posterior	−43.8 ± 79.4	−5.3 ± 12.7	0.020	
L2-3 abdominal	−177.6 ± 220.1	−12.5 ± 12.5	0.002	
L2-3 anterior	−79.2 ± 72.2	−13.3 ± 11.1	<0.001	0.522
L2-3 posterior	−98.3 ± 166.0	−11.7 ± 14.4	0.016	
L3-4 abdominal	−171.5 ± 204.4	−11.8 ± 12.4	0.001	
L3-4 anterior	−56.9 ± 90.2	−8.9 ± 14.9	0.011	0.010
L3-4 posterior	−114.6 ± 129.9	−13.3 ± 13.4	0.001	
L4-5 abdominal	−253.2 ± 404.0	−8.8 ± 17.7	0.011	
L4-5 anterior	−69.9 ± 140.3	−5.8 ± 19.3	0.038	0.009
L4-5 posterior	−183.3 ± 277.2	−10.3 ± 17.9	0.008	
L5-caudal abdominal	−499.8 ± 264.0	−9.4 ± 4.8	<0.001	
L5-caudal anterior	−220.2 ± 241.7	−9.7 ± 11.2	0.001	0.382
L5-caudal posterior	−279.5 ± 142.5	−9.3 ± 4.4	<0.001	

Table 2
VAT changes around organs and in different regions (L1-2, L2-3, L3-4, L4-5, L5-caudal). The p-value indicates statistically significant differences between baseline and follow-up VAT around the corresponding organ or in the different regions.

ΔVAT	absolute [cm^3]	relative [%]	p-value
abdominal	−647.1 ± 325.9	−15.2 ± 6.5	<0.001
left kidney	−53.5 ± 85.0	−9.6 ± 15.4	0.011
right kidney	−73.1 ± 89.1	−11.9 ± 13.6	0.002
spleen	−82.3 ± 110.7	−16.5 ± 20.8	0.004
pancreas	−5.2 ± 148.5	−7.2 ± 43.6	0.874
other	−461.2 ± 323.1	−16.1 ± 8.9	<0.001
L1-2	−83.6 ± 69.3	−15.6 ± 12.6	<0.001
L2-3	−80.9 ± 74.8	−14.2 ± 12.9	<0.001
L3-4	−52.5 ± 94.4	−8.9 ± 19.6	0.022
L4-5	−39.2 ± 67.5	−8.6 ± 15.7	0.018
L5-caudal	−82.7 ± 105.3	−10.9 ± 14.0	0.002

Table 3
Changes of organ volume of liver, left and right kidney, spleen, and pancreas. The p-value indicates statistically significant differences between baseline and follow-up value of the corresponding parameter.

	liver	left kidney	right kidney	spleen	pancreas
Δ organ volume [cm^3]	−258.2 ± 214.9	−13.1 ± 29.1	−9.1 ± 21.3	−2.6 ± 85.2	1.1 ± 47.9
Δ organ volume [%]	−13.6 ± 11.1	−5.0 ± 14.2	−3.8 ± 12.0	−0.8 ± 27.7	15.3 ± 68.8
p-value	<0.001	0.059	0.070	0.892	0.917

2.3. Abdominal organ segmentation

2.3.1. Generation of segmentations for atlases

19 MRI datasets, considered as atlases, were randomly selected from the 40 MRI datasets and it was assured that the selected datasets were coming from different patients. Manual segmentation was performed by one operator to generate segmentations for 19 atlases using the experimental image analysis software package 3D-Slicer [24]. The following quantitative endpoints were obtained: volumes of liver, left/right kidney, spleen, pancreas, as well as annotations of vertebral body locations.

2.3.2. Data preprocessing

The input data was downsampled in order to reduce computational complexity introduced by the group-wise diffeomorphic registration. The preprocessing steps therefore included: (a) removal of the background, (b) removal of the artifacts from MRI acquisition (water-fat swaps at the edge of the FOV in the left-right direction) using morphological operations, (c) removal of the abdominal skin (only keeping abdominal cavity and structures within it) using morphological operations and (d) down-sampling of the data from the reconstruction voxel size of $0.98 \times 0.98 \times 5\,\text{mm}^3$ to that of $3 \times 4 \times 7.5\,\text{mm}^3$.

2.3.3. Multi-atlas segmentation

For image segmentation a multi-atlas approach was adopted. In this approach a number of manually annotated image volumes were assumed to be available. If a new volume had to be annotated, all of the annotated image volumes were registered to the new case. The resulting transforms were used to also transfer the annotations to the coordinate space of the new volume, and all transformations were fused.

Volume registration started with an affine registration resulting in an initial global alignment, and followed by a diffeomorphic transformation for finer alignment. In a previous study, a method using both water and fat images for intra-subject registration was developed [22]. However, the registration between patient and atlas datasets required larger deformation than that between intra-subject datasets, resulting in much larger transformation complexity and higher computational cost. In consideration of computational efficiency, only the water data was used in the proposed work for the abdominal organ segmentation.

The Advanced Normalization Tools [25] was used for the image registration. It provides an open source software library for image normalization [25] and enabled multiple transformation abilities with adjustable level of complexity (ANTs was freely available at http://stnava.github.io/ANTs/). The parameters set in ANTs were: Affine deformation (4 level image pyramid with each level 10000 iterations at most) with a Mutual Information similarity measure (32 bins and 16000 samples) was firstly applied for global alignment. A diffeomorphic registration was then performed using cross-correlation similarity measure (weight 1, window 5). It has been reported that diffeomorphic transformations perform well in the presence of large deformation fields [25,26]. The ANTs framework was implemented in MATLAB and took approximately 20 min of computation time per registration on a computer with Intel Core i5 1.3 GHz processor, 8GB 1600 MHz DDR3 memory.

After all annotations had been transformed to the coordinate space of new target volume, the transformed annotations were fused. In this step, the selective and iterative method for performance level estimation (SIMPLE) [27] was employed for averaging. First, a fused segmentation ground truth from all of the transformed annotations was generated using majority voting. Subsequently, the SIMPLE algorithm evaluated the Dice coefficient between the initial fused segmentation and each transformed annotations. Inputs with a Dice value smaller than a threshold were discarded. A specific threshold was computed at each iteration i according to the equation $\tau_i = \mu_i^{Dice} - \sigma_i^{Dice}$, where μ and σ were the mean and standard deviation of the Dice values of all input annotations at this iteration. The remaining annotations were fused in a weighted averaging with the Dice coefficient values serving as weights. The above procedure was iterated until there was no annotation being discarded.

2.3.4. Flow chart of abdominal organ segmentation approach

Fig. 1 shows the steps of the proposed segmentation algorithm. Step (I) included the manual generation of 19 atlases. Step (II) included the procedure of registration-based segmentation. Each of preprocessed atlas dataset was co-registered with the preprocessed patient dataset. The output deformation field then transformed segmentations of interested organs to the patient spatial coordinate system. The registration consisted of affine and diffeomorphic deformation provided by the ANTs framework. In this way, a group of normalized segmentation labels was automatically yielded. Step (III) included the label fusion method—SIMPLE that fused the normalized and resampled segmentation labels to compute the final segmentation.

The algorithm was applied on all 40 datasets and automatically segmented the aforementioned previously annotated abdominal organs. When the algorithm annotated an MRI dataset, which was from the same patient as one of the atlases datasets, the corresponding atlas dataset was discarded.

2.4. Adipose tissue measurement

The organ segmentation and morphological operations were used to develop the algorithm for automatic measurement of adipose tissues. The adipose tissue measurement algorithm was implemented in MATLAB and took around 3 min for the adipose tissue classification and measurement on a computer with Intel Core i5 1.3 GHz processor, 8GB 1600 MHz DDR3 memory.

2.4.1. SAT and VAT measurement

SAT can be found under the skin and VAT is located within the abdominal cavity. The center of vertebral bodies was used to separate SAT into anterior and posterior components. Specifically, SAT was classified as anterior SAT (located anterior to the center of the vertebral bodies) and posterior SAT (located posterior to the center of the vertebral bodies). In addition, the volume of VAT, anterior and posterior SAT can be computed in the blocks of L1-L2, L2-L3, L3-L4, L4-L5 and L5-downward in 10 cm.

Fig. 2 shows the flow chart of the employed fat classification algorithm. K-means clustering was used to classify the adipose tissue within the abdomen, and morphological operations further separated AAT into VAT and SAT. With the use of vertebral bodies, SAT could be classified as anterior SAT and posterior SAT and all SAT and VAT compartments were computed in different regions across the feet/head direction using the blocks of L1-L2, L2-L3, L3-L4, L4-L5 and L5-downward in 10 cm.

2.4.2. Organ-specific adipose tissue measurement

The organ segmentations were used to measure organ-specific VAT, as shown in Fig. 2. An Euclidean distance transformation was applied on each organ for marking the VAT around the organ within 5 cm as organ-specific VAT, automatically creating, in this way, a VAT distribution map. The VAT volume within 5 cm from the periphery of the kidneys, the spleen and the pancreas were determined.

2.5. Statistical analysis

The statistical analysis was performed using SPSS (SPSS 22.0, Chicago, IL, USA). All tests were performed based on a 0.05 level of significance. Mean and standard deviation (SD) of all parameters at baseline and follow-up as well as the absolute and relative change over time (Δ = follow-up—baseline and Δ = (follow-up—baseline)/baseline) were computed over the 20 subjects. The Kolmogorov-Smirnov test showed for all parameters no significant difference from a normal distribution ($p > 0.05$). Therefore, changes over time were evaluated with paired t-tests.

3. Results

The ANTs registration method (using greedy symmetric diffeomorphism as transformation model and cross correlation as similarity metric) presented acceptable performance for organ segmentation on 40 datasets before performing the label fusion step. The final segmentation label of interested organ was generated by label fusion method (SIMPLE) fusing a set of normalized labels. The Dice coefficients between the manual and the final automatic segmentation (after the label fusion) were 0.943 ± 0.023 on liver, 0.894 ± 0.052 on left kidney, 0.873 ± 0.063 on right kidney, 0.855 ± 0.091 on spleen and 0.672 ± 0.155 on pancreas. Fig. 3 illustrates a representative organ segmentation result: axial, coronal and sagittal views from one subject before (A) and after (B) undergoing dietary intervention are shown, using different colors for labeling five of the automatically segmented organs.

Fig. 4(A) and (B) shows the same axial slice from one representative subject before and after diet, respectively. The reduction of anterior SAT, posterior SAT and VAT volumes can be easily recognized and measured, meanwhile, the change of organ-specific VAT volumes—5 cm around interested organ—was tracked. The axial slices in Fig. 5 show the segmentation of kidney-specific VAT and VAT not around any organs of one subject before and after performed dietary intervention.

The changes of different types of AAT after weight loss were subsequently analyzed. A statistically significant reduction of abdominal SAT was observed after four weeks ($-1518.7 \pm 632.8\,cm^3$, $-10.8\% \pm 4.2\%$, $p < 0.001$). SAT changes for all regions and compartments were statistically significant ($p < 0.05$) as shown in Table 1. Abdominal ΔSAT were significantly greater in the posterior than the anterior compartment ($-11.4\% \pm 5.1\%$ versus $-9.5\% \pm 6.3\%$, $p < 0.001$, Table 1). Particularly, the posterior L3-L4 and L4-L5 ΔSAT were significantly greater than those in the corresponding anterior

regions ($p < 0.05$). The other regions showed no statistically significant difference between the anterior and posterior compartment ($p > 0.05$, Table 1). Furthermore, SAT changes were greater in the L2-L3 ($-12.5\% \pm 12.5\%$) and L3-L4 ($-11.8\% \pm 12.4\%$) region and less pronounced in the L1-L2 region ($-6.6\% \pm 13.5\%$) (Fig. 6). However, the latter differences were not statistically significant ($p > 0.05$).

Abdominal VAT decreased after four weeks ($-647.1 \pm 325.9\,cm^3$, $-15.2\% \pm 6.5\%$, $p < 0.001$). Except for VAT around the pancreas, reductions of VAT were statistically significant ($p < 0.05$; Table 2). VAT loss located not around any organ ($-16.1\% \pm 8.9\%$) was statistically significant greater than those around liver, left and right kidney, spleen, and pancreas ($p < 0.001$, Table 2). The regional VAT loss from L1-L2 to L5-caudal was not significantly different ($p > 0.05$, Table 2).

A statistically significant reduction in organ volume was only found for the liver ($-258.2 \pm 214.9\,cm^3$, $-13.6\% \pm 11.1\%$, $p < 0.001$, Table 3).

4. Discussion

The present work proposed a novel fully automatic method for abdominal organ segmentation and abdominal adipose tissue regional analysis and quantification. The results from the automatic method showed very good agreement with the manually created references for organ segmentation. The developed automatic algorithm allowed the detection of SAT and VAT subcompartments changes in a study of 20 obese women undergoing a calorie restriction intervention [3].

Previous studies have presented semiautomatic or fully automatic methods for the classification of adipose tissue. However, most of previous studies were limited to segmentation approaches focusing exclusively on the measurement of abdominal SAT and VAT [3,4] and did not investigate SAT and VAT subcompartments. Joshi et al. showed the feasibility of using a registration-based approach for the segmentation of adipose tissue and liver [22], but the developed method was only applicable to longitudinal studies in which manually segmented labels at baseline data could be only propagated to the same subject's dataset scanned in future time points [22]. The presently proposed automatic method was able to classify SAT and VAT subcompartments in a few minutes without human interaction, and the multi-atlas-based segmentation method provided a fully automatic way to segment abdominal organs with high accuracy. The combination of the registration-based approach with label fusion prevented the bad labels generated by occasional failed registration from making final segmentation decision. Voting fusion strategies have been commonly used to produce robust segmentations. Especially, weighted voting method has provided significant improvement in segmentation accuracy [28]. In contrast to majority voting method, the SIMPLE method remarkably improves the segmentation accuracy by taking atlas selection and performance estimation strategies into account. The performance estimation strategies result in discarding the badly performing segmentations in each iteration. The remaining segmentations, which have good segmentation performance, are used to yield the final segmentation.

Some previous studies have used thresholding to differentiate between abdominal adipose tissue and non-fat tissue from T1-weighted images [4]. The MRI datasets used in the present work were water- and fat-separated images from chemical encoding-based technique. Compared to T1-weighted images, the employed Dixon technique provided co-registered water- and fat-separated abdominal images enabling the separation of fat tissue from abdominal water tissues and the development of an automatic method analyzing fat depots. The water-separated images were used as an input to the organ segmentation part of the algorithm and both the water- and fat-separated images were used as an input to the adipose tissue measurement and classification part of the algorithm.

The SAT and VAT volumes were greatly decreased after weight loss in the studied 20 obese patients. Distinct changes were also observed for different SAT and VAT compartments. Abdominal SAT reduction was significantly greater in posterior than the anterior compartment. This observation is consistent with a previously study showing that AAT changes were more significantly linked to the posterior than the anterior SAT changes [9]. The above observation on SAT changes could be related to the fact that posterior SAT contains a larger component of deep SAT than anterior SAT does. In addition, we found that the significant difference between posterior and anterior SAT changes originates primarily from changes at L3-4 and L4-5 regions. Moreover, the reduction of abdominal VAT was statistically significant, however, the regional VAT loss from L1-2 to L5-caudal was not significantly different. The VAT loss located not around any organ was significantly greater than the VAT loss around liver, left and right kidney, spleen, and pancreas, suggesting that VAT in the anterior part of the body is the most mobile VAT depot after dietary intervention. The above observation on VAT changes could be related to the fact that VAT located not around any organ would be primarily composed from intraperitoneal fat, whereas the other presently studied VAT compartments would include also parts of retroperitoneal fat.

A reduction in liver volume was also presently observed. It is established that the liver fat reduction is strongly related to weight loss and it has been shown that weight loss is also associated with reduction in total liver volume and liver fat fraction [29]. In addition, there has been recent work using water-fat imaging and measuring the total fat volume by integrating the liver fat fraction over the entire liver volume [12]. Therefore, the present work is consistent with previous studies. However, a multi-echo sequence using more than two echoes and accounting for known confounding factors (including T2* decay effects) would be required in order to measure liver proton density fat fraction and assess liver fat volume changes.

The current study presents a novel automatic method for the assessment of adipose tissue and the segmentation of abdominal organs, but it has certain limitations. Firstly, in comparison to other abdominal organs, the segmentation of pancreas was less accurate. This is likely due to the fact that the pancreas is small in volume and it is, therefore, difficult to differentiate the pancreas from the surrounding visceral fat. Secondly, the present analysis included intramuscular and paravertebral fat in visceral adipose tissue. The ratio of the above two fat components to abdominal VAT in obese subjects is small. However, the above two components have to be excluded from abdominal VAT, when the methodology is applied to leaner subjects. Thirdly, the present analysis did not extract the traditional SAT compartments (deep and superficial) and the traditional VAT compartments (retroperitoneal and intraperitoneal). The extraction of the above compartments would require the localization of the fascia lata and the peritoneum, which was not possible with the present data. Instead geometrically meaningful compartments were defined: for SAT based on the vertebral body location and for VAT based on the organ location. Fourthly, the filling status of the bowel can affect the VAT regional assessment. Fifthly, the present methodology was only tested in obese subjects. Finally, the employed methodology used two-point Dixon imaging and could not model $T_2{}^*$ decay effects in the quantification of the fat fraction. The last limitation can be easily overcome by using a water-fat signal model with a single $T_2{}^*$ correction in an acquisition with more than 2 echoes (typically six), in order to quantify the desired proton density fat fraction [30].

5. Conclusion

The present work introduced a fully automatic method for organ segmentation and adipose tissue regional assessment based on abdominal water and fat MRI images. The algorithm's performance showed a very good agreement on organ segmentation with the manually created reference and enabled the assessment of different SAT and VAT subcompartments changes after a dietary intervention in obese women.

Conflict of interest

The authors declare the following conflicts of interest: H. Kooijman is an employee of Philips Healthcare and D. C. Karampinos receives grant support from Philips Healthcare.

Grant support

The present study was supported by funding of Philips Healthcare (to DCK), the German Federal Ministry of Education and Research (BMBF, FKZ: 01EA1329, to HH), the Technische Universitat Munchen—Institute for Advanced Study (funded by the German Excellence Initiative and the European Union Seventh Framework Programme under grant agreement n 291763, to BHM) and the Marie Curie COFUND program of the European Union (Rudolf Mossbauer Tenure- Track Professorship to BHM).

References

[1] M. Takahara, I. Shimomura, Metabolic syndrome and lifestyle modification, Rev. Endocr. Metab. Disord. 15 (4) (2014) 317–327.
[2] K. Kantartzis, J. Machann, F. Schick, K. Rittig, F. Machicao, A. Fritsche, H.U. Haring, N. Stefan, Effects of a lifestyle intervention in metabolically benign and malign obesity, Diabetologia 54 (4) (2011) 864–868.
[3] C. Cordes, M. Dieckmeyer, B. Ott, J. Shen, S. Ruschke, M. Settles, C. Eichhorn, J.S. Bauer, H. Kooijman, E.J. Rummeny, T. Skurk, T. Baum, H. Hauner, D.C. Karampinos, MR-detected changes in liver fat, abdominal fat, and vertebral bone marrow fat after a four-week calorie restriction in obese women, J. Magn. Reson. Imaging 42 (5) (2015) 1272–1280.
[4] J. Machann, C. Thamer, N. Stefan, N.F. Schwenzer, K. Kantartzis, H.U. Haring, C.D. Claussen, A. Fritsche, F. Schick, Follow-up whole-body assessment of adipose tissue compartments during a lifestyle intervention in a large cohort at increased risk for type 2 diabetes, Radiology 257 (2) (2010) 353–363.
[5] M.C. Mojtahedi, M.P. Thorpe, D.C. Karampinos, C.L. Johnson, D.K. Layman, J.G. Georgiadis, E.M. Evans, The effects of a higher protein intake during energy restriction on changes in body composition and physical function in older women, J. Gerontol. A Biol. Sci. Med. Sci. 66 (11) (2011) 1218–1225.
[6] W. Shen, J. Chen, M. Gantz, G. Velasquez, M. Punyanitya, S.B. Heymsfield, A single MRI slice does not accurately predict visceral and subcutaneous adipose tissue changes during weight loss, Obesity (Silver Spring) 20 (12) (2012) 2458–2463.
[7] Q. He, E.S. Engelson, D.P. Kotler, A comparison of abdominal subcutaneous adipose tissue pattern in obese and lean HIV-infected women, J. Nutr. 135 (1) (2005) 53–57.
[8] D.E. Kelley, F.L. Thaete, F. Troost, T. Huwe, B.H. Goodpaster, Subdivisions of subcutaneous abdominal adipose tissue and insulin resistance, Am. J. Physiol. Endocrinol. Metab. 278 (5) (2000) E941–E948.
[9] A. Misra, A. Garg, N. Abate, R.M. Peshock, J. Stray-Gundersen, S.M. Grundy, Relationship of anterior and posterior subcutaneous abdominal fat to insulin sensitivity in nondiabetic men, Obes. Res. 5 (2) (1997) 93–99.
[10] N. Abate, A. Garg, R. Coleman, S.M. Grundy, R.M. Peshock, Prediction of total subcutaneous abdominal, intraperitoneal, and retroperitoneal adipose tissue masses in men by a single axial magnetic resonance imaging slice, Am. J. Clin. Nutr. 65 (2) (1997) 403–408.
[11] C.J. Hsieh, P.W. Wang, T.Y. Chen, The relationship between regional abdominal fat distribution and both insulin resistance and subclinical chronic inflammation in non-diabetic adults, Diabetol. Metab. Syndr. 6 (1) (2014) 49.
[12] A. Tang, J. Chen, T.A. Le, C. Changchien, G. Hamilton, M.S. Middleton, R. Loomba, C.B. Sirlin, Cross-sectional and longitudinal evaluation of liver volume and total liver fat burden in adults with nonalcoholic steatohepatitis, Abdom. Imaging 40 (1) (2015) 26–37.
[13] H.H. Hu, H.E. Kan, Quantitative proton MR techniques for measuring fat, NMR Biomed. 26 (12) (2013) 1609–1629.
[14] H.H. Hu, J. Chen, W. Shen, Segmentation and quantification of adipose tissue by magnetic resonance imaging, MAGMA (2015), http://dx.doi.org/10.1007/s10334-015-0498-z.
[15] J. Kullberg, J. Brandberg, J.E. Angelhed, H. Frimmel, E. Bergelin, L. Strid, H. Ahlstrom, L. Johansson, L. Lonn, Whole-body adipose tissue analysis: comparison of MRI, CT and dual energy X-ray absorptiometry, Br. J. Radiol. 82 (974) (2009) 123–130.
[16] P. Ranefall, A.W. Bidar, P.D. Hockings, Automatic segmentation of intra-abdominal and subcutaneous adipose tissue in 3D whole mouse MRI, J. Magn. Reson. Imaging 30 (3) (2009) 554–560.
[17] S.A. Sadananthan, B. Prakash, M.K. Leow, C.M. Khoo, H. Chou, K. Venkataraman, E.Y. Khoo, Y.S. Lee, P.D. Gluckman, E.S. Tai, S.S. Velan, Automated segmentation of visceral and subcutaneous (deep and superficial) adipose tissues in normal and overweight men, J. Magn. Reson. Imaging 41 (4) (2015) 924–934.
[18] M.S. Thomas, D. Newman, O.D. Leinhard, B. Kasmai, R. Greenwood, P.N. Malcolm, A. Karlsson, J. Rosander, M. Borga, A.P. Toms, Test-retest reliability of automated whole body and compartmental muscle volume measurements on a wide bore 3T MR system, Eur. Radiol. 24 (9) (2014) 2279–2291.
[19] A. Valentinitsch, D.C. Karampinos, H. Alizai, K. Subburaj, D. Kumar, T.M. Link, S. Majumdar, Automated unsupervised multi-parametric classification of adipose tissue depots in skeletal muscle, J. Magn. Reson. Imaging 37 (4) (2013) 917–927.
[20] D. Wald, B. Teucher, J. Dinkel, R. Kaaks, S. Delorme, H. Boeing, K. Seidensaal, H.P. Meinzer, T. Heimann, Automatic quantification of subcutaneous and visceral adipose tissue from whole-body magnetic resonance images suitable for large cohort studies, J. Magn. Reson. Imaging 36 (6) (2012) 1421–1434.
[21] B.T. Addeman, S. Kutty, T.G. Perkins, A.S. Soliman, C.N. Wiens, C.M. McCurdy, M.D. Beaton, R.A. Hegele, C.A. McKenzie, Validation of volumetric and single-slice MRI adipose analysis using a novel fully automated segmentation method, J. Magn. Reson. Imaging 41 (1) (2015) 233–241.
[22] A.A. Joshi, H.H. Hu, R.M. Leahy, M.I. Goran, K.S. Nayak, Automatic intra-subject registration-based segmentation of abdominal fat from water-fat MRI, J. Magn. Reson. Imaging 37 (2) (2013) 423–430.
[23] H. Eggers, B. Brendel, A. Duijndam, G. Herigault, Dual-echo Dixon imaging with flexible choice of echo times, Magn. Reson. Med. 65 (1) (2011) 96–107.
[24] S. Pieper, M. Halle, R. Kikinis, 3D slicer, biomedical imaging: nano to macro, IEEE Int. Sym. (2004).
[25] B.B. Avants, N.J. Tustison, G. Song, P.A. Cook, A. Klein, J.C. Gee, A reproducible evaluation of ANTs similarity metric performance in brain image registration, Neuroimage 54 (3) (2011) 2033–2044.
[26] J. Ashburner, A fast diffeomorphic image registration algorithm, Neuroimage 38 (1) (2007) 95–113.
[27] T.R. Langerak, et al., Label fusion in atlas-based segmentation using a selective and iterative method for performance level estimation (SIMPLE), medical imaging, IEEE Trans. 29 (12) (2010) 2000–2008.
[28] X. Artaechevarria, A. Munoz-Barrutia, C. Ortiz-de-Solorzano, Combination strategies in multi-atlas image segmentation: application to brain MR data, IEEE Trans. Med. Imaging 28 (8) (2009) 1266–1277.
[29] N.S. Patel, I. Doycheva, M.R. Peterson, J. Hooker, T. Kisselva, B. Schnabl, E. Seki, C.B. Sirlin, R. Loomba, Effect of weight loss on magnetic resonance imaging estimation of liver fat and volume in patients with nonalcoholic steatohepatitis, Clin. Gastroenterol. Hepatol. 13 (3) (2015) 561–568.
[30] S.B. Reeder, I. Cruite, G. Hamilton, C.B. Sirlin, Quantitative assessment of liver fat with magnetic resonance imaging and spectroscopy, J. Magn. Reson. Imaging 34 (4) (2011) 729–749.